Instantaneous Incremental Current-Based Faulted Phase Selection Algorithm

Jagannath Wijekoon, Athula. D. Rajapakse

***Abstract*-- A novel, simple and fast method to identify the faulted phases using the maximum rate of change of incremental current (ROCOIC) is proposed. Six indices are calculated considering a pairwise comparison of ROCOIC. The decision-making process is based on selecting which two indices are the largest among all. The algorithm requires only three thresholds to detect fault inception and to identify the ground and three-phase faults. Simulation studies show that the method is robust and not affected by fault inception angle, fault location, and fault resistance. The proposed method only requires locally measured current signals. Since the method relies on the fundamental component of instantaneous incremental current, the proposed method can be implemented in systems with low sampling rates and avoids the need to use transducers with high bandwidth.**

***Keywords*: Phase selection, faulted phase selection, instantaneous incremental current, fault classification.**

I. Introduction

PROMPT and accurate fault type classification and faulted phase selection schemes play a major role in the protection of transmission lines. A properly implemented phase selection scheme should (i) allow the faulted loops in the distance relay to operate while blocking the healthy loops and (ii) enable single-pole tripping and reclosing schemes by differentiating single-phase faults from multi-phase faults. With the growing penetration of inverter-based resources (IBR), the inertia of power systems is reduced, and strict stability margins are introduced to maintain the system stability. Therefore, critical clearing times are reduced and the faults in the system must be cleared faster. Hence faulted phase selection schemes must operate within a short time window after the inception of a fault to ensure the prompt and correct operation of protection schemes.

Faulted phase selection schemes can be categorized into three groups: i) phasor-based methods; ii) superimposed component-based methods [1], [2]; iii) transient component-based methods [3]. Phasor-based phase selection algorithms typically take at least one cycle to make a decision. If the HV circuit breaker operating time of 2-3 cycles is considered [4], the typical fault clearance time would be in the range of 3 – 4.5 cycles after considering the time of 1-1.5 cycles [4] to issue a trip signal of phasor-based methods. This can create unfavorable system conditions in a system with strict stability margins and short critical clearing times. Some of the incremental component-based phase selection algorithms [1], [2] have shown improvements in speed and accuracy, but they are still based on the phase angle relationships between the fault currents and voltages.

Hence, transient-based faulted phase selection algorithms have been proposed as a solution to the limitations faced by phasor-based faulted phase selection algorithms. Most of these transient-based methods typically use the wavelet transform to extract transients from fault-generated signals [3], [5] – [8] and often use machine learning methods such as neural networks, fuzzy logic, decision trees, and support vector machines to develop the phase selection algorithm [5], [9] – [13]. In addition to machine learning-based methods, threshold-based methods that use fault-induced transients are also reported in the literature [14] – [16]. These transient-based methods are capable of identifying faulted phases in less than a millisecond reducing the relay decision-making time by a significant margin.

Even though transient-based faulted phase selection algorithms show promising results some drawbacks are inherent to transient-based methods. One of the major drawbacks of transient-based methods is the effect of fault inception angle. A fault in a transmission line generates a step change in the voltage profile and this step change generates the transients. The strength of these transients is mainly dependent on the size of the step change in voltage. The size of the step change is determined by the fault inception angle and the fault resistance. Hence, if a high resistance fault occurs closer to the zero crossing of the voltage waveform, the transient-based algorithms are vulnerable to producing incorrect results or failing to operate completely. This drawback is common to almost all transient-based schemes. Another drawback of transient-based methods is the dependency on high sampling rates. Typically, most of the transient-based scheme focuses on high-frequency transients ranging from a few kHz to several MHz range. Therefore, sampling rates of these transients-based methods vary from kHz to MHz range [3], [5] based on the considered frequency ranges of the algorithms. Hence to implement some of these proposed methods, special transducers with high bandwidth or signal processing modules with special capabilities may require increasing the cost. The accuracy of transient-based methods can be affected by the traveling wave reflections at transposition points and joints of

Jagannath Wijekoon and Athula. D. Rajapakse are with Department of Electrical and Computer Engineering, University of Manitoba, R3T 3X8 Canada (e-mail of corresponding author: wiwmigjs@myumanitoba.ca).

Paper submitted to the International Conference on Power Systems Transients (IPST2023) in Thessaloniki, Greece, June 12-15, 2023.

non-homogeneous line segments. In addition to that, the transient-based methods which utilize machine learning-based techniques often require large sets of data to train the models which come at a high engineering cost.

The concept of using derivatives of currents for protection, fault location, and faulted conductor identification is not new and it has been used in HVDC systems. These methods in the published literature mainly use the transient part of the current waveform, and when this concept is applied to AC transmission systems they face major challenges as mentioned above. This paper extends some initial ideas of [14] – [16] to overcome many of the drawbacks discussed above and proposes a novel, simpler, fast, and robust phase selection algorithm. This new algorithm uses incremental currents in a way that is completely different from the algorithms proposed in [1], [2]. Six indices are defined as ratios of the rate of change (ROC) of instantaneous incremental currents of different pairs of phase currents. Each of these indices reflects relative magnitudes of the rate of change of incremental current through the two phases considered.

The novelty of the proposed method is as follows. Unlike the methods using transient portions of the derivatives of currents, the method proposed in this paper uses the derivate of instantaneous incremental currents. The incremental currents used in the proposed method is low pass filtered such that the frequency spectrums of the incremental currents do not contain high-frequency transient currents. Therefore, the impact of the fault inception angle is minimized in the proposed instantaneous incremental current-based method.

The proposed method has many advantages. Since the proposed method only relies on local current measurements the proposed method does not need to use voltage transducers or communication schemes. The method makes decisions based on the relative magnitudes of the calculated indices. Therefore, the method does need any threshold settings except for a threshold setting to identify the three-phase fault and a threshold setting to discriminate ground fault. This reduces the need to run intensive system studies to determine threshold settings and reduces the overall complexity of the algorithm. Since the proposed method only requires the fundamental frequency component of incremental current, unlike most transient-based phase selection methods which require high sampling rates in the range of hundreds of kHz, the proposed method can be implemented with sampling rates used in conventional relay platforms. In addition, the use of incremental currents reduces the effect of load currents and the non-homogeneity of lines.

The rest of the paper is organized as follows. Section II describes the principle behind the proposed method. Section III describes the signal processing involved in the proposed algorithm and explains the complete implementation of the algorithm. The proposed incremental current-based phase selection method is evaluated in Section IV and Section V presents the conclusions.

II. Principle Behind Incremental Current-Based Phase Selection Scheme

A. Incremental Quantities

Incremental quantities presumably consist of only the fault-induced components of voltages and currents and are intuitively understood as the differences between the fault voltage and currents and their pre-fault values. However, the term "Incremental Quantities" is a broad term, and based on the filtering frequency range three types of incremental quantities can be defined. These are i) Instantaneous incremental quantities, (ii) Phasor incremental quantities, and (iii) High-frequency incremental quantities.

Phasor incremental quantities only contain the fundamental frequency component of the fault component, and it comes at the expense of the filter latency and slower operation whereas high-frequency incremental components are obtained using high pass filtering and are short-lived. On the other hand, instantaneous incremental quantities contain all the frequency components including the decaying dc component, the fault component of the fundamental frequency, and the high-frequency transients. This paper uses instantaneous incremental quantities after conditioning to focus on a narrow band around the fundamental frequency.

B. Instantaneous Incremental Current Based Faulted Phase Selection Indices

When a fault occurs in a transmission line, fault currents start to flow in the phases involved in the fault. Therefore, current magnitudes in the faulted phase or phases are significantly higher than the current magnitudes in the non-faulted phase or phases. However, trying to identify the faulted phase or phases using a simple magnitude comparison would not be successful under high resistance faults or when the system is heavily loaded. Since incremental currents observed in the post-fault current represent the fault-induced components, the process of identifying faulted phases becomes much simplified. Therefore, a pairwise comparison of the rate of change of (ROCOC) incremental currents is used to identify the strength of the incremental currents, and the likely source of incremental currents can be identified.

This paper proposes the pair of indices defined in (1) to compare two phases; thus, for a three-phase system, six indices can be calculated.

$$F_{xy} = \frac{\max\left|\frac{d\Delta i_x(t)}{dt}\right|}{\max\left|\frac{d\Delta i_y(t)}{dt}\right|} \quad F_{yx} = \frac{\max\left|\frac{d\Delta i_y(t)}{dt}\right|}{\max\left|\frac{d\Delta i_x(t)}{dt}\right|} \qquad (1)$$

This index is a measure of the relative strength of the incremental current to another phase and vice versa where $\Delta i_x(t)$ and $\Delta i_y(t)$ are instantaneous incremental currents of phase-X and -Y respectively. The absolute maximum rate of change of incremental currents within a short time window of length T_w is used for computing the indices. Ground faults are identified by checking for the existence of zero sequence currents.

C. Faulted Phase Identification Using the Proposed Indices

The following three subsections describe the basis of criteria to identify the faulted phases.

1) Identifying the Faulted Phase in Phase-to-Ground Faults

Consider a Phase-A-to-Ground fault. During this fault, a significant incremental current can be observed in Phase-A and little to no incremental currents can be observed in Phases B and C. Hence the six indices during a Phase-A-to-Ground fault would have the following relationships: $F_{ab} \gg 1$, $F_{bc} \approx 1$, $F_{ca} \ll 1$, $F_{ba} \ll 1$, $F_{cb} \approx 1$, and $F_{ac} \gg 1$. Therefore, during a Phase-to-Ground fault, the two indices which have the faulted phase incremental current as the numerator will be the largest two indices among six indices while the other four indices will be a) Approximately equal to one or b) Less than one.

Thus, the following logic can be used to determine the faulted phase in any Phase-to-Ground fault.

$$\begin{aligned} &if\{(max(F_{ab},F_{bc},F_{ca}) = F_{ab}) \ \&(max(F_{ba},F_{cb},F_{ac}) \\ &= F_{ac})\}: AG\ Fault \\ &else\ if\{(max(F_{ac},F_{bc},F_{ca}) = F_{bc}) \ \&(max(F_{ba},F_{cb},F_{ac}) \\ &= F_{ba})\}: BG\ Fault \\ &else\ if\{(max(F_{ab},F_{bc},F_{ca}) = F_{ca}) \ \&(max(F_{ca},F_{cb},F_{ac}) \\ &= F_{cb})\}: CG\ Fault \end{aligned} \quad (2)$$

2) Identifying the Faulted Phases in Phase-to-Phase and Phase-to-Phase-to-Ground Faults

To explain the logic to identify the phases in Phase-to-Phase or Phase-to-Phase-to-Ground faults, consider a Phase-B-to-C fault. During a Phase-B-to-C fault, significant incremental currents can be observed in Phases-B and -C. Hence the six indices during a Phase-B-to-C fault would be related as: $F_{ab} \ll 1$, $F_{bc} \approx 1$, $F_{ca} \gg 1$, $F_{ba} \gg 1$, $F_{cb} \approx 1$, and $F_{ac} \ll 1$. In general, during a Phase-to-Phase or Phase-to-Phase-to-Ground fault, the two indices which have the incremental currents of the faulted phases in the numerator will be the largest two indices while the other four indices will be either less than one or approximately equal to one. Hence, a logic scheme can be developed to identify the faulted phases in Phase-to-Phase and Phase-to-Phase-to-Ground faults.

$$\begin{aligned} &if\{(max(F_{ab},F_{bc},F_{ca}) = F_{bc}) \ \&(max(F_{ba},F_{cb},F_{ac}) \\ &= F_{ac})\}: AB/ABG\ Fault \\ &else\ if\{(max(F_{ab},F_{bc},F_{ca}) = F_{ab}) \ \&(max(F_{ba},F_{cb},F_{ac}) \\ &= F_{cb})\}: AC/ACG\ Fault \\ &else\ if\{(max(F_{ab},F_{bc},F_{ca}) = F_{ca}) \ \&(max(F_{ba},F_{cb},F_{ac}) \\ &= F_{ba})\}: BC/BCG\ Fault \end{aligned} \quad (3)$$

Phase-to-Phase-to-Ground faults can be discriminated from the Phase-to-Phase faults by checking the existence of zero sequence currents.

3) Identifying Three-Phase Faults

During a Three-Phase fault, incremental currents can be observed in all three phases. Therefore, all six indices will be approximately equal to one. Hence, the difference between the index and its inverse index should be theoretically equal to zero. The logic to identify the Three-Phase faults is given in (4).

$$\begin{aligned} &if\{(|F_{ab} - F_{ba}| < k_1) \ \&(|F_{bc} - F_{cb}| < k_1) \ \&\ (|F_{ca} - F_{ac}| \\ &< k_1)\}: Three - Phase\ Fault \end{aligned} \quad (4)$$

The threshold k_1 can safely be set to 1.

The criteria to identify the faulted phases can be summarized in Table 1 where the largest two indices out of the six calculated indices during a fault are marked by an X.

TABLE 1 LARGEST TWO INDICES FOR DIFFERENT FAULT TYPES

Fault	Index					
	F_{ab}	F_{bc}	F_{ca}	F_{ba}	F_{cb}	F_{ac}
AG	X					X
BG		X		X		
CG			X		X	
AB/ABG		X				X
AC/ACG	X				X	
BC/BCG			X	X		

III. SIGNAL PROCESSING AND ALGORITHM IMPLEMENTATION

As mentioned in Section II. A. , instantaneous incremental currents consist of all the frequency components including the decaying dc component, the fundamental frequency component of the fault component, and high-frequency components. The proposed phase selection scheme works best when focused on the fundamental frequency component of the fault component. To eliminate dc components and high-frequency noise due to traveling waves, some amount of signal conditioning is required. The signal processing involved in the proposed algorithm is depicted in Fig. 1 along with the index calculation stage. Fig.1 (a) shows the signal processing and maximum value calculation stage of the algorithm. The instantaneous current samples are first filtered using a digital mimic filter to remove the decaying dc component. Accurate knowledge of the system-dependent filter time constant is not critical for this application. Upon removing the dc component, the current samples are low-pass filtered to remove the high-frequency transients. Incremental currents are calculated after the filtering stage using the equation given in (5).

$$\Delta i(n) = i(n) - i(n - kN) \quad (5)$$

where *k* is the delay in number of cycles and *N* is the number of samples per cycle.

Fig.1 (b) shows the fault detection logic and the index calculation stage of the algorithm. Until the fault is detected the indices are forced to 1. Once the fault is detected, the timer is activated. The value of the index at the end of the timer is held at the sample & hold circuit. A simple threshold-based comparison method is employed to detect the fault condition in this paper and it works fast and reliably for a variety of conditions. If desired, any other robust fault detection technique can be used.

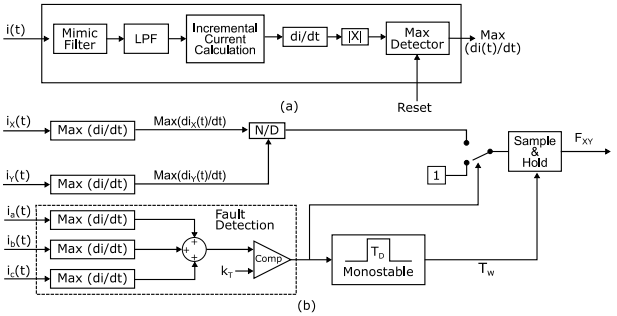

Fig.1 Calculating the Faulted Phase Identification Indices (a) Signal Conditioning and Max(di/dt) detector, (b) Index calculation

Fig. 2 shows the complete phase selection algorithm. Once the fault is detected, first the three-phase fault check is carried out to identify the existence of a three-phase fault. Then the ground faults are discriminated by checking for the existence of zero

sequence current by comparing the zero-sequence current against threshold k_0. Then the logic conditions for each fault are checked until a decision is made.

IV. Algorithm Evaluation

A. Test System

The algorithm was evaluated using the 230 kV power system shown in Fig. 3, simulated in the electromagnetic transient (EMT) simulation program PSCAD/EMTDC™.

The sources were modeled as voltage sources with different positive and zero sequence impedances. The two sources are connected to the system using Δ-Y grounded transformers. The three-phase transformer model available in the transformer library was used to model the two transformers. The transmission lines were modeled using frequency-dependent line models available in PSCAD/EMTDC transmission line library with default settings. The 3-conductor delta tower type was used, and the line design is shown in Fig. 3(a). Chukar conductors having a DC resistance of 0.0203 Ω/km and a radius of 0.032m were used for phase conductors. The DC resistance and radius of ground conductors are 2.8645 Ω/km and 0.0055m respectively. The transmission lines were transposed by connecting three-line segments as shown in Fig. 4 instead of enabling ideal transposition. The ground plane component available in the transmission library in PSCAD/EMTDC™ was used to represent the earth ground return path of the system and it was approximated with a constant resistivity of 100 Ωm. The current transformer (CT) was modeled using the JA model and the potential transformer (PT) was modeled using the Lucas model available in the protection library in PSCAD/EMTDC™ simulation software with ratios of 500:5 and 230000:115 for CT and PT respectively. The parameters of the transmission line at 50 Hz are given in

Table 2. The source impedances are given in

Table 3. The parameters of the CT and PT models are given in

Table 4 and

Table 5. Parameters of the three-phase transformer are given in

Table 6. The faults were modeled as two-state resistances (1 MΩ no-fault, 0.01 Ω short circuit). The simulation was run with 10 μs time steps.

The three-threshold settings and the low pass filter cutoff frequency were verified through a simulation study. Low pass filter cutoff frequency was selected such that the filter removes a sufficient amount of transients with minimum filter delay. Therefore, the low pass filter cutoff frequency was set to 150 Hz. This cutoff frequency works well for systems with 50 or 60 Hz nominal frequency, but the value of the cutoff frequency is not critical as long as high-frequency content is removed. The fault detection threshold (k_T) should be set above the absolute sum of peak di/dt values under normal operation, which is theoretically equal to zero since no incremental currents should be flowing in the circuit during a non-fault situation. Hence, the threshold setting was set to 1 A/s. In practice, this threshold can be adjusted during the commissioning so that it does not trigger due to normally present noise. The setting is also not critical, as it is not required for the faulted phase selection algorithm to discriminate between faults and other events (such as load or line switching, etc.). The ground fault discrimination threshold (k_0) was set to 5 % of the steady state RMS current to 0.1125 A. The three-phase fault detection threshold (k_1) was set to 1.0. The index calculation time window (T_w) was set to 5 ms. A window length of about a quarter cycle ensures a fast response and minimizes any influence of CT saturation because, in properly designed systems, it is highly unlikely for DC saturation to occur in the first quarter cycle after a fault. The signal conditioning and algorithm parameters can be fine-tuned to a given system, for example, k_0 can be set more sensitively for systems with high impedance or resonance grounding.

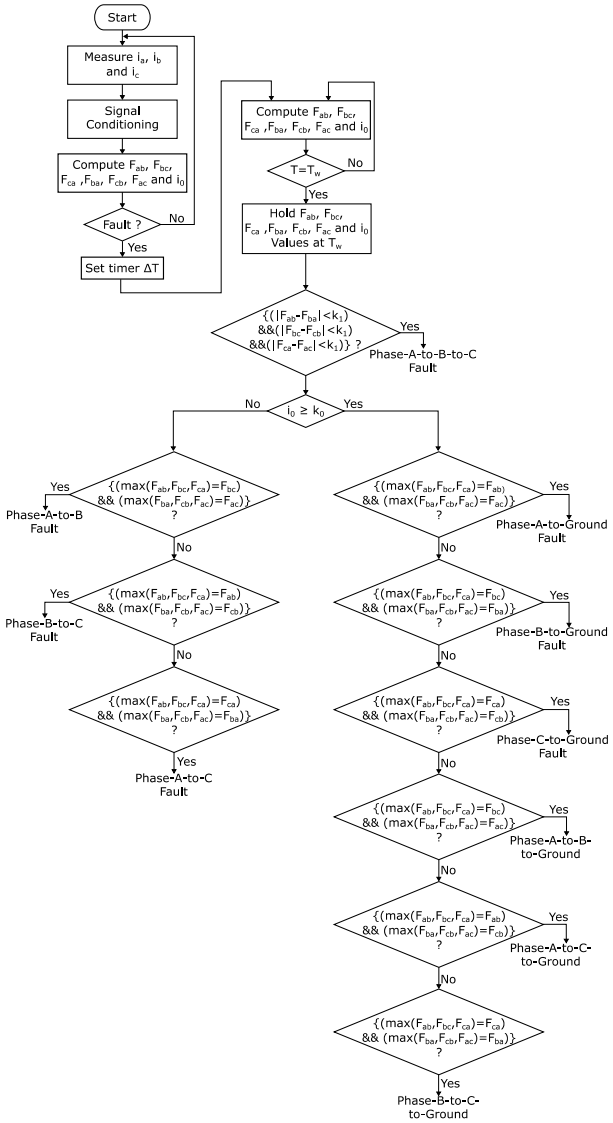

Fig. 2 Incremental Current-Based Faulted Phase Selection Algorithm

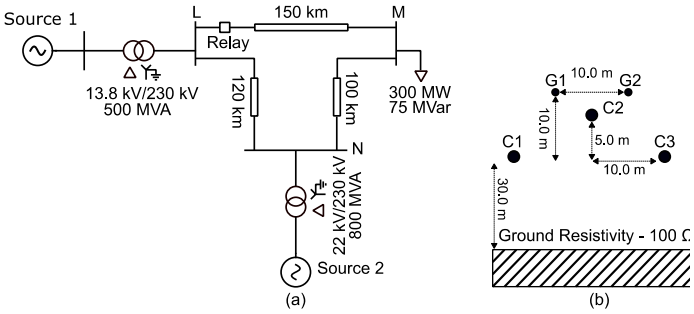

Fig. 3 (a) Test System and (b) Transmission Line Design

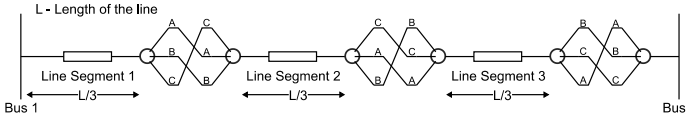

Fig. 4 Line Transposition Scheme

TABLE 2 TRANSMISSION LINE PARAMETERS (230 KV, 100 MVA BASE)

Parameter	Value (p.u)	Parameter	Value (p.u)
R_1	0.0098	R_0	0.0851
X_1	0.1200	X_0	0.3240

TABLE 3 SOURCE IMPEDANCE DATA

Source	Z_1 (Ω)	Z_0 (Ω)	MVA
Source 1	$1.077\angle 87.65^o$	$0.896\angle 80.86^o$	500
Source 2	$0.15125\angle 89.9^o$	$0.0725\angle 89.9^o$	800

TABLE 4 CURRENT TRANSFORMER PARAMETERS

Parameter	Value
Primary Turns / Secondary Turns	240
Secondary Resistance / Inductance	0.5 Ω / 0.8×10^{-3} H
Core Area	2.601×10^{-3} m^2
Burden Resistance / Inductance	0.5 Ω / 0.8×10^{-3} H

TABLE 5 POTENTIAL TRANSFORMER PARAMETERS

Parameter	Value
Primary Resistance/Inductance (on secondary)	0.05 Ω / 0.47×10^{-3} H
Secondary Resistance/Inductance	0.18 Ω / 0.47×10^{-3} H
Hysteresis/Eddy Current Loss	5.0 W / 2.5 W
Secondary Operating Voltage/Frequency	115 V/50 Hz
Operating Flux Density	0.8 T
Burden Resistance/Inductance – Series	301.0 Ω/2.4 H
Burden Resistance – Parallel	785.0 Ω

TABLE 6 TRANSFORMER DATA

Parameter	Value	
	Transformer 1	Transformer 2
Line-to-Line Voltages: Winding -1/Winding -2	13.8 kV/230 kV	22 kV/230 kV
Transformer MVA	500	800
Positive Sequence Leakage Reactance	0.1 p.u	0.1 p.u
Magnetizing Current	2.0 %	2.0 %
Air Core Reactance/Knee Voltage	0.2 p.u / 1.17 p.u	0.2 p.u / 1.17 p.u

B. Demonstration of Basic Algorithm

TO DEMONSTRATE THE BASIC OPERATION OF THE PROPOSED ALGORITHM, FAULTS LISTED IN Table 7 were applied in the middle of Line-LM at 0.5 s.

TABLE 7 CONSIDERED FAULT SCENARIOS

Scenario	Fault	Fault Resistance	Location
Scenario-1	BG	150 Ω	50 % of Line LM
Scenario-2	AC	150 Ω	50 % of Line LM
Scenario-3	ABC	150 Ω	50 % of Line LM

Fig. 5 shows the rate of change of incremental currents (ROCOIC) for considered fault scenarios. Fig. 5 (a) shows the ROCOIC for Scenario-1 where the ROCOIC of phase-B is significantly larger than the ROCOIC of the other two phases. In addition to that, variations of ROCOIC of phases-A and C are identical during the fault scenario. Hence, F_{ba} and F_{bc} will be much larger than F_{ab}, F_{ca}, F_{cb}, and F_{ab} which satisfies the condition given in (2). Similar behavior can be observed for other Phase-to-Ground faults as well.

Fig. 5 (b) depicts the variation of ROCOIC for fault Scenario-2. The ROCOIC of the two faulted phases (Phase-A and C) are much larger than the non-faulted phase (Phase-B). Since the magnitude variation of the two faulted phases is identical, F_{ca} and F_{ac} indices would be approximately equal to one whereas F_{ab}, and F_{cb} would be much larger than the other four indices. Hence, using the logic given in (3) the two faulted phases can be identified as Phase-A and C. A similar kind of behavior can be observed in a Phase-A-to-Phase-C-to-Ground fault scenario as well. The only difference would be the existence of zero sequence current.

Fig. 5 (c) shows the variation of ROCOIC for fault Scenario 3. In this case, all three phases show a significant amount of incremental currents compared to the other two fault scenarios. Furthermore, the magnitude variation of all three phases is similar to each other. Therefore, all six indices calculated during this fault scenario would be close to one satisfying the criteria given in (4).

Table 8 shows the index values for the considered fault scenarios. Even with a high fault resistance value such as 150 Ω the proposed method can identify the correct faulted phase which is one of the main advantages of the proposed algorithm.

TABLE 8 INDEX VALUES FOR CONSIDERED FAULT SCENARIOS

Scenario	F_{ab}	F_{bc}	F_{ca}	F_{ba}	F_{cb}	F_{ac}
Scenario-1	0.096	9.73	1.07	10.41	0.10	0.934
Scenario-2	77.62	0.013	0.99	0.013	77.62	1.00
Scenario-3	0.877	1.34	0.85	1.14	0.74	1.18

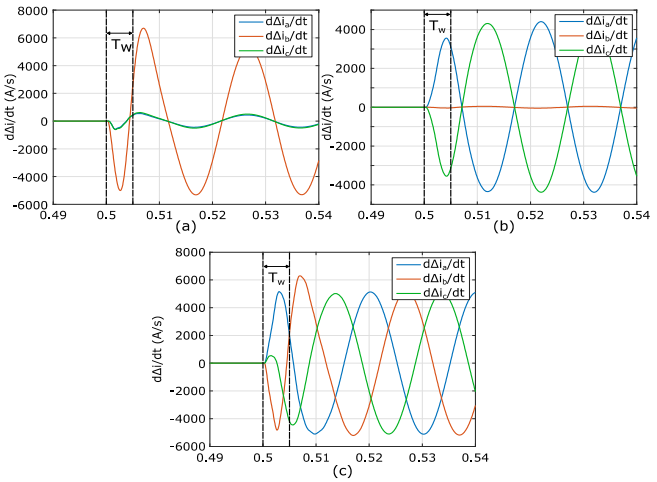

Fig. 5 Rate of Change of Incremental Currents for (a) Scenario-1, (b) Scenario-2, and (c) Scenario-3

C. Identification of Phase-to-Ground Faults

Fig. 6 shows the variation of fault indices for Phase-C-to-Ground fault for three different fault resistances (0.01 Ω, 100 Ω, and 300 Ω). Fault inception angle was varied in one-degree steps from zero to 180 degrees. The faults were applied at 50 % of the length of Line-LM. Irrespective of the fault resistance value, the indices F_{ca} and F_{cb} remains the largest two indices while F_{ab} and F_{ba} are close to one and F_{ac} and F_{bc} remains the smallest indicating a Phase-C-to-Ground fault. The results prove the robustness of the proposed algorithm against the fault resistance and inception angle, some of the weaknesses that transient-based phase selection algorithms such as those proposed in [14]–[16] had.

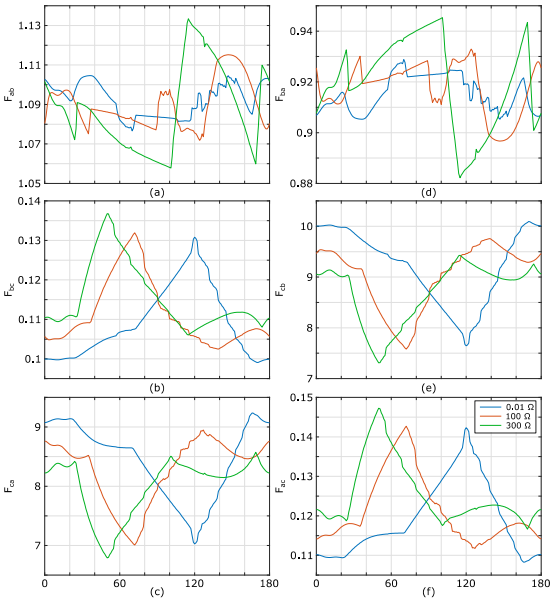

Fig. 6 Variation of Fault Indices with Fault Inception Angle for Three Fault Resistances for Phase C-G faults (a) F_{ab}, (b) F_{bc}, (c) F_{ca}, (d) F_{ba}, (e) F_{cb}, and (f) F_{ac}

The influence of fault location on the proposed algorithm was analyzed by applying Phase-A-to-Ground short circuit faults on Line-LM between 10 % and 100 % of the line length. Fig. 7 depicts the variation of fault indices with 1-degree increments along the line. The indices F_{ab} and F_{ac} which are depicted in Fig. 7 (a) and Fig. 7 (f) remain as the two largest indices irrespective of the fault inception angle and fault location verifying the existence of a Phase-A-to-Ground fault.

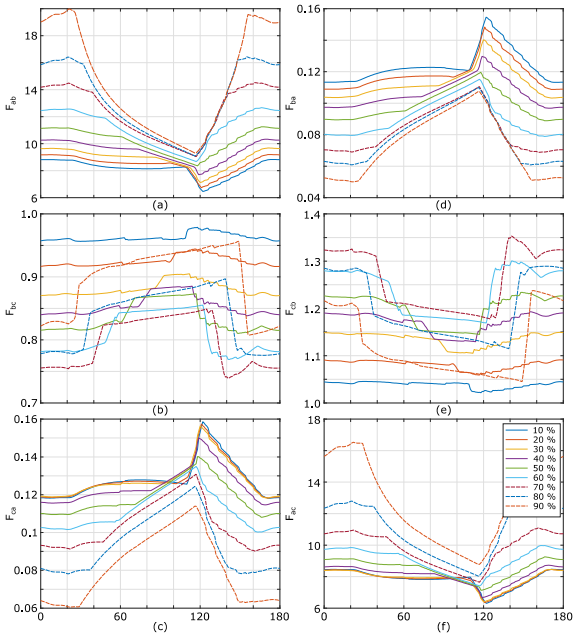

Fig. 7 Variation of Fault Indices (a) F_{ab}, (b) F_{bc}, (c) F_{ca}, (d) F_{ba}, (e) F_{cb}, and (f) F_{ac} with Location for Phase-A-G fault

D. Identification of Phase-to-Phase Faults

Fig. 8 depicts the variation of fault indices for Phase-A-to-C fault applied at 80 % of line length with fault inception angle for three different fault resistances (0.01 Ω, 100 Ω, and 300 Ω). The fault indices F_{ab} and F_{cb} remains as the two largest fault indices irrespective of the fault resistance and fault inception angle to verify the existence of Phase-A-to-C fault. For all three considered fault resistance values, F_{ab} and F_{cb} values vary within the same range which shows that the proposed method has a minimal effect from fault resistance.

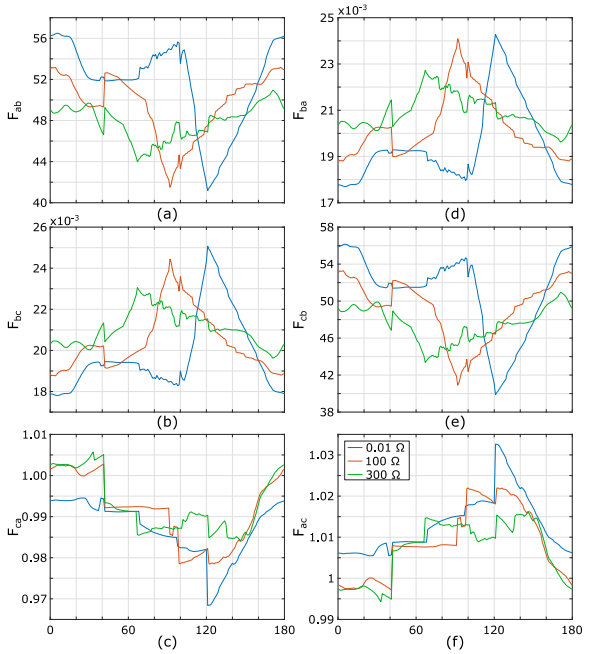

Fig. 8 Variation of Fault Indices with Fault Inception Angle for Three Different Fault Resistances for Phase A-C fault (a) F_{ab}, (b) F_{bc}, (c) F_{ca}, (d) F_{ba}, (e) F_{cb}, and (f) F_{ac}

Fig. 9 depicts the variation of fault indices for Phase-A-to-B short circuit faults applied on the Line-LM between 10 % and

100 % of the line length. The fault inception angle was incremented in 1-degree steps. Irrespective of the fault location, indices F_{bc} and F_{ac} remains the two largest indices verifying the existence of Phase-A-to-B fault irrespective of the fault location

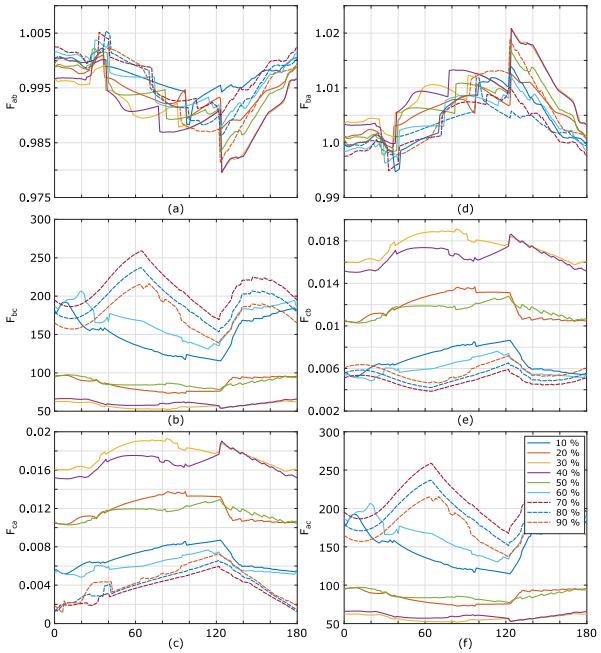

Fig. 9 Variation of Fault Indices (a) F_{ab}, (b) F_{bc}, (c) F_{ca}, (d) F_{ba}, (e) F_{cb}, and (f) F_{ac} with Location for Phase A-B fault

E. Identification of Phase-to-Phase-to-Ground Faults

Fig.11 depicts the variation of fault indices for Phase-B-to-C-to-Ground short circuit faults applied on the Line-LM between 10 % and 100 % of line length. The zero sequence current component confirms it is a ground fault as shown in Fig. 10. Then F_{ba} and F_{ca} remains the two largest indices irrespective of the fault location and the fault inception angle, verifying the existence of a phase B-to-C-to-Ground fault.

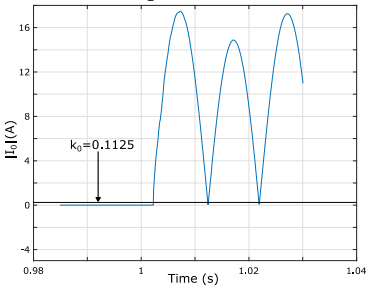

Fig. 10 Variation of Zero Sequence Current During Phase-B-C-G Fault

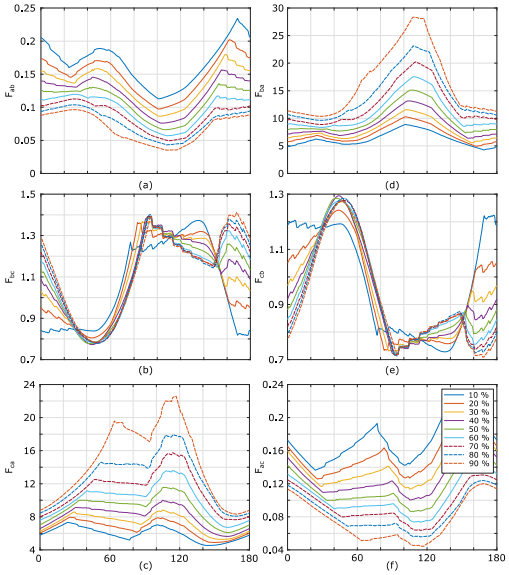

Fig. 11 Variation of Fault Indices (a) F_{ab}, (b) F_{bc}, (c) F_{ca}, (d) F_{ba}, (e) F_{cb}, and (f) F_{ac} with the location for Phase-B-C-G fault.

F. Three Phase Faults

The variation of Three-Phase fault detection indices ($|F_{ab}-F_{ba}|$, $|F_{bc}-F_{cb}|$, and $|F_{ca}-F_{ac}|$) for a Three-Phase fault applied at 90 % of the line length at three different fault resistances (0.01 Ω, 100 Ω, and 300 Ω) is depicted in Fig. 12. The algorithm is capable of identifying Three-Phase faults at least up to faults with 100 Ω fault resistance irrespective of the fault inception angle. Results not shown due to page limitation confirmed that the algorithm is able to identify the three-phase fault irrespective of the fault location up to 100 Ω fault resistance.

At 300 Ω fault resistance, the proposed algorithm fails to identify the three-phase fault within an approximate fault inception angle window of 100 degrees. This is due to the filter transients introduced by the mimic filter at fault inception angles where no decaying dc component is present. This can be alleviated by blocking the index calculation for a specific time period. However, this would come at the cost of speed.

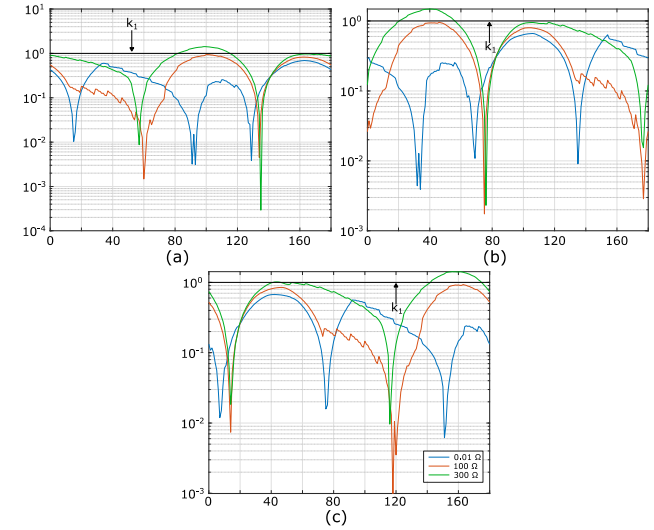

Fig. 12 Variation of Three Phase Detection Threshold with Increasing Fault Resistance (a) $|F_{ab}-F_{ba}|$, (b) $|F_{bc}-F_{cb}|$, and (c) $|F_{ca}-F_{ac}|$ for Three-Phase Faults Applied at 90 % Line Length

G. Results for a System with IBR

To investigate the performance of the proposed method on a system with IBR, the system shown in Fig. 3 (a) was modified by replacing source 1 with a Type-IV 125 MW wind farm model [17] and opening the line MN. For the grid-side converter, the d-axis control mode was set to V_{dc} control and the q-axis control model was set to Q control mode with priority set to I_q control during ride-through conditions. Whereas in the machine side converter, the d-axis control mode was set to P control and the q-axis control mode was set to V_{ac} control and the priority was set to I_d control. The same threshold settings and filter parameters defined in Section IV. A. were used in the algorithm. Phase-to-Ground and Phase-to-Phase faults were applied at 90 % of the length of Line-LM were applied with a fault resistance of 50 Ω. The index values for each fault type are given in Table 9. The proposed algorithm was able to correctly identify the faulted phases in the applied faults.

With line MN open, the fault current contribution from the synchronous source was gradually reduced by changing the source strength and the faulted phase selection performance for a 50 Ω line-ground fault at 90% of line L-M was evaluated repeatedly. When the fault current is supplied predominantly from the wind farm (i.e. the fault current contribution from the synchronous source is less than 5%), the proposed method was unable to correctly identify the faulted phases. This is due to lack of significant incremental currents present in the faulted phases as a result of the control actions of the IBR controls. This is a limitation of the proposed method when protecting a radial line fed only from an IBR.

TABLE 9 FAULT INDEX VALUES FOR EACH FAULT TYPE IN A SYSTEM WITH IBR

Fault	F_{ab}	F_{bc}	F_{ca}	F_{ba}	F_{cb}	F_{ac}
AG	5.39	1.4	0.13	0.19	0.73	7.44
BG	0.14	8.26	0.87	7.17	0.12	1.1
CG	1.36	0.1	7.06	0.74	9.6	0.16
AB	1.02	21.2	0.05	0.98	0.05	21.63
AC	13.5	0.08	0.93	0.07	12.62	1.07
BC	0.076	0.96	13.73	13.13	1.05	0.073

V. CONCLUSIONS

This paper proposes a simple and novel faulted phase selection scheme based on a set of indices determined using the peak rate of change of incremental currents. The results show that the proposed method is not affected by fault inception angle, fault resistance, and fault location and is applicable for both transposed and non-transposed transmission lines. The proposed faulted phase selection scheme only requires three threshold settings and is much faster than phasor-based faulted phase selection schemes. The decision-making time which is constrained by time window and filter delays is less than 6 ms. Even though it is slower than transient-based methods the proposed method is more reliable compared to transient-based methods. However, the proposed method fails to operate correctly in fault scenarios where the fault current is purely supplied from IBRs due nonexistence of significant incremental currents.

VI. REFERENCES

[1] G. Benmouyal and J. Roberts, "Superimposed Quantities: Their True Nature and Application in Relays," *26th Annual Western Protective Relay Conference*, pp. 1–18, 1999.

[2] G. Benmouyal and J. Mahseredjian, "A combined directional and faulted phase selector element based on incremental quantities," *IEEE Transactions on Power Delivery*, vol. 16, no. 4, pp. 478–484, Oct. 2001.

[3] X. Dong, W. Kong, and T. Cui, "Fault classification and faulted-phase selection based on the initial current traveling wave," *IEEE Transactions on Power Delivery*, vol. 24, no. 2, pp. 552–559, 2009.

[4] R. Abboud and D. Dolezilek, "Time-Domain Technology – Benefits to Protection, Control, and Monitoring of Power Systems," in *International Conference and Exhibition – Relay Protection and Automation for Electric Power Systems*, 2017, no. April, pp. 1–8.

[5] A. Abdullah, "Ultrafast Transmission Line Fault Detection Using a DWT-Based ANN," *IEEE Trans Ind Appl*, vol. 54, no. 2, pp. 1182–1193, 2018.

[6] Z. He, L. Fu, S. Lin, and Z. Bo, "Fault detection and classification in EHV transmission line based on wavelet singular entropy," *IEEE Transactions on Power Delivery*, vol. 25, no. 4, pp. 2156–2163, 2010.

[7] F. Shwe Myint and W. Wichakool, "Fault Type Identification Method based on Wavelet Detail Coefficients of Modal Current Components; Fault Type Identification Method based on Wavelet Detail Coefficients of Modal Current Components," in *2018 IEEE 5th International Conference on Smart Instrumentation, Measurement and Application (ICSIMA)*, 2018, pp. 1–6.

[8] J. A. Jiang, P. L. Fan, C. S. Chen, C. S. Yu, and J. Y. Sheu, "A Fault Detection and Faulted-Phase Selection Approach for Transmission Lines with Haar Wavelet Transform," in *Proceedings of the IEEE Power Engineering Society Transmission and Distribution Conference*, 2003, vol. 1, pp. 285–289.

[9] N. S. D. B. Silva, K. M., B. A. Souza, "Fault Detection and Classification in Transmission Line Using Wavelet Transform and ANN," *IEEE Transactions on Power Delivery*, vol. 21, no. 4, pp. 2058–2063, 2006.

[10] N. W. A. Lidula and A. D. Rajapakse, "A pattern recognition approach for detecting power islands using transient signals - Part I: Design and implementation," *IEEE Transactions on Power Delivery*, vol. 25, no. 4, pp. 3070–3077, 2010.

[11] P. Jafarian and M. Sanaye-Pasand, "High-frequency transients-based protection of multiterminal transmission lines using the SVM technique," *IEEE Transactions on Power Delivery*, vol. 28, no. 1, pp. 188–196, 2013.

[12] H. Livani and C. Y. Evrenosoglu, "A fault classification method in power systems using DWT and SVM classifier," in *Proceedings of the IEEE Power Engineering Society Transmission and Distribution Conference*, 2012.

[13] H. Livani and C. Y. Evrenosoglu, "A fault classification and localization method for three-terminal circuits using machine learning," *IEEE Transactions on Power Delivery*, vol. 28, no. 4, pp. 2282–2290, 2013.

[14] M. N. Haleem and A. D. Rajapakse, "A Transient Based Phase Selection Method for Transmission Line Protection," in *International Conference on Power System Transients*, 2019, pp. 1–6.

[15] J. Wijekoon, A. D. Rajapakse, and N. M. Haleem, "Fast and Reliable Method for Identifying Fault Type and Faulted Phases Using Band Limited Transient Currents," *IEEE Transactions on Power Delivery*, vol. 36, no. 5, pp. 2839–2850, Oct. 2021.

[16] J. S. Wijekoon, M. N. Haleem, and A. D. Rajapakse, "Transient based faulted conductor selection method for double circuit lines," *Electric Power Systems Research*, vol. 196, Jul. 2021.

[17] "Knowledge Base | PSCAD." https://www.pscad.com/knowledge-base/article/227 (accessed Oct. 19, 2022).